Journal of Chemical Health Risks

www.jchr.org

JCHR (2024) 14(5), 861-866 | ISSN:2251-6727

Rapid Synthesis and Physiochemical Characterization of Aluminium-Oxide Nanoparticles via Citric Acid Facilated Auto Combustion Synthesis

Gajendra Singh Lodhi[1], Jyoti Sharma[1*], Laxman Singh[2] and Atendra Kumar[3]

[1]Department of Chemistry, School of Basic and Applied Sciences, Shobhit Institute of Engineering and Technology (Deemed-to-be-University), Meerut, UP., India- 250110.

[2]Department of chemistry, Siddharth University, Kapilvastu, Siddharth Nagar, UP., India- 272202.

[3]Department of Chemistry, Simdega College (A constituents unite of Ranchi University), Simdega-835223. Jharkhand., India.

(**Received:**14 June 2024 **Revised:** 01 July 2024 **Accepted:** 18 August 2024)

KEYWORDS
Al_2O_3 NPs, XRD, W-H plot, TGA, SEM, combustion synthesis.

ABSTRACT:

Introduction: In order to manufacture of Al_2O_3 nanoparticles for this study, we used the Sol-Gel approach. The resulting NPs were then calcined at 1350°C for 3 hours. The phase stability and the crystal arrangement of the NPs were determined using X-ray diffraction analysis and this investigations demonstrate the formation of hexagonal structure (Space Group: R-3c) with the lattice constant a=b= 4.761 Å and c= 12.978Å, respectively. The thermal stability and the heat flow of Al_2O_3 nanoparticles were investigated through TG-DSC curve. The presence of deformed shape of the grains with unclear grain boundaries were observed from the SEM and cross-sectional SEM micrograph. The average grain size obtained through the SEM analysis and estimated to be 1.01 µm on the scale of 1 µm using Image J software, which was justified with the help of Histogram curve. The EDS results confirmed the existence of Al, O elements in alumina nanoparticles with Atomic (%) (32.48 % of Al, 67.52 %of O) and weight (%) (44.79 % of Al, 55.20 % of O) suggesting the purity of the synthesized NPs.

1. Introduction

A lot of thought has been focused on the potential use of ultrafast and small sized single metal-oxide powders as structural and functional materials for mechanical and electrical components. The most significant classes of nanoparticles today and in the near future are simple oxides, such as aluminum oxide (class of porous nanomaterials) with the chemical formula Al_2O_3 also termed as alumina that assemble as corundum-like structure with six oxygen atoms around one aluminum atom, are employed in well-established applications [1,2]. Nanoparticles of aluminum oxide have comparable handling and accessibility characteristics as other metal oxide nanoparticles (NPs). In addition, these affordable nanoparticles have a large surface area, strong mechanical properties, low electrical conductivity, remarkable thermal and chemical stability, high melting point, and abrasive environments. Applications for it may be found in the medical fields, the microelectronics industry, material science, engineering, and other fields [3, 4]. Moreover, due to possession of large surface area of these nanoparticles can be used as starting materials for sintering and molding of oxide materials for practical purposes. The crystalline structure and physical and chemical characteristics allow for it to be found in numerous trends that diverge from one another in addition to its widely utilized in refractories, abrasives, microelectronics, catalysis, and structural applications. In particular, premium corundum polycrystalline materials find application as bearings in watches and other high-precision devices, as well as electronic substrates [5]. It was one of the most significant engineering materials due to its special qualities such as chemical stability, a high melting point, and high hardness etc in the late of 20th century. These qualities allowed for a wide range of applications, most notably in optics, the production of ceramics and refinement [6-8]. There are several phases in which alumina may occur of which the phases like α and γ –alumina is two of the most significant phases among them. Bohemite heat treatment at 1000 °C results in the formation of the alpha phase which is a thermodynamically stable phase with a number of characteristics, including high hardness, chemical stability, and thermal stability with melting point around 2051 °C. This makes it possible to employ it in the production of ceramic shields, protective coatings, and ceramics [9]. Conversely, phase α can be achieved by applying

Journal of Chemical Health Risks

www.jchr.org

JCHR (2024) 14(5), 861-866 | ISSN:2251-6727

heat treatment between 600 and 700 °C, converting the unstable phase known as γ –alumina phase. It serves as a medium in chemical processes, however it shouldn't be utilized at high temperatures since it turns into the α phase around 950 °C [10]. Different techniques such as decomposition, exploding wire, laser ablation, sol-gel, solution reduction gas evaporation, mechanical ball milling, and mechano-chemical processes was employing straightforward and affordable protocols, can be used to synthesize Al NPs. They also include liquid, gas phase, and gas phase-based synthesis techniques [11, 12]. Furthermore, Sol-gel method is the most advantageous and extensively used method other than above mentioned methods for synthesis of Al NPs because it provides good control over the stoichiometry and shape of nanoparticles and produces low raw material cost, high thermal stability, low synthesis temperature, high purity along with specific surface area of solid particles [13-16].

In the recent research work, ultrafine α-Al_2O_3 powders have been developed through a rather easy, effective, and inexpensive aqueous sol-gel approach based on the in situ synthesis of water soluble metal complexes using aluminum nitrate and citric acid as raw ingredients. Investigations are conducted on the shape of the produced alumina powder, phase changes, and the breakdown of the citrate precursor.

1. Material Synthesis

The Al_2O_3 nanoparticles was created through sol-gel precursor route by using analytical grade chemicals, Al(III) nitrate, $Al(NO_3)_3.9H_2O$ (sigma Aldrich, 99.9 %) and citric acid, $C_6H_8O_7H_2O$ (99% Merck, India) as raw materials. In a beaker, the appropriate amount of double-distilled water was added to create a homogenous solution containing the stoichiometry number of copper ions (Al^{3+}) and the solutions were subsequently incorporated with the equivalent of one metal's worth of citric acid. Up until it transformed into a hours at 60 ºC yellowish sol, the solution was continually swirled for a few hours at 60 ºC.

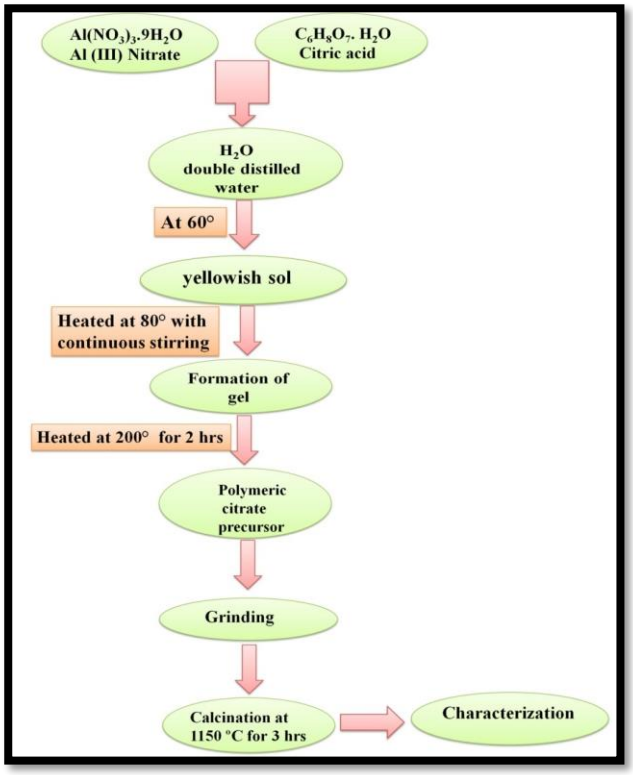

Fig. 1. Flow chart for synthesis of Al_2O_3 nanoparticles through sol-gel precursor route.

After that, the stabilized nitrate-citrate solution was heated quickly to 80 ºC while being continuously agitated. The sol transformed itself into a translucent stick gel, changing its color and viscosity. A puffy, polymeric citrate precursor was obtained by heating the gel to 200 ºC for 2 hours. Finely, an electrical furnace was used to calcine Al_2O_3 nanoparticles at 600 ºC for 5 hours in the air after grinding the precursor to a fine powder. After then, the 2wt.% of PVA was mixed with the calcined Al_2O_3 particles and shaped into cylindrical pellets using a hydraulic press, heated at 350 ºC for 2 hrs for removing of PVA as binder from pellets and it was used for different physiochemical characterizations.

2. Material characterization

The crystal structures of the samples were studied by Cu-Ka radiation (40 kV, 60 mA) -based X-ray diffraction (XRD) with the model of Rigaku D/max-2400 and diffraction data were collected over the 2θ range of 20°–80°. The scan rate of 1 deg/min and step size of 0.02° step size was used for the measurement. Granulated Al_2O_3 powders were used for thermal gravimetric analysis (TGA) and

Journal of Chemical Health Risks

www.jchr.org

JCHR (2024) 14(5), 861-866 | ISSN:2251-6727

differential scanning calorimetry (DSC) using a NETZSCH instrument of the model STA 449 F3, which was operated at 10 ◦C/min from room temperature to 1300 ◦C. Alumina particles were mounted on carbon tape using the Cressington Sputter 108 Auto Coater, which then applied a 20 nm thick layer of gold coating to them. The microstructures were analyzed using a scanning electron microscope SEM, JEOL JSM-6390A, Japan with a secondary electron detector that was operating at a distance of 14.5 mm and electron energy of 20.0 kV. The SEM-EDS (Energy Dispersive Spectroscopy) experiment was carried out using the SEM, JEOL JSM-6390A, Japan with the EDAX, Inc. EDS detector and EDX; Kevex, Sigma KS3software. The spectra were obtained at 14.5 mm working distance and 20.0 kV accelerating voltage. The conductive carbon tape was covered in alumina particles prior to examination and spectrum data was collected on a 150 x 150 µm zone that was covered with particles.

2-theta(deg)	d (ang.)	FWHM(deg)	Crystallite size(nm)	Plane corresponding Corundum phase
25.638	3.4717	0.119	7.13	(0 1 2)
35.203	2.54729	0.123	7.06	(1 0 4)
37.823	2.37662	0.120	7.29	(1 1 0)
43.398	2.08334	0.135	6.60	(1 1 3)
52.596	1.73864	0.146	6.34	(0 2 4)
57.535	1.60055	0.159	5.96	(1 1 6)
59.766	1.5460	0.150	6.37	(2 1 1)
61.363	1.50957	0.238	4.06	(1 2 2)
66.550	1.40393	0.159	6.23	(2 1 4)
68.244	1.37315	0.163	6.14	(3 0 0)
77.274	1.23366	0.203	5.23	(1 1 9)

Table- The values of average crystallite of Al_2O_3 NPs calculated using Eq. (1).

3. Results and discussion

Powder XRD analysis was used for investigating at the Al_2O_3 nanoparticles phase development and crystal structure, as shown in Fig.2.

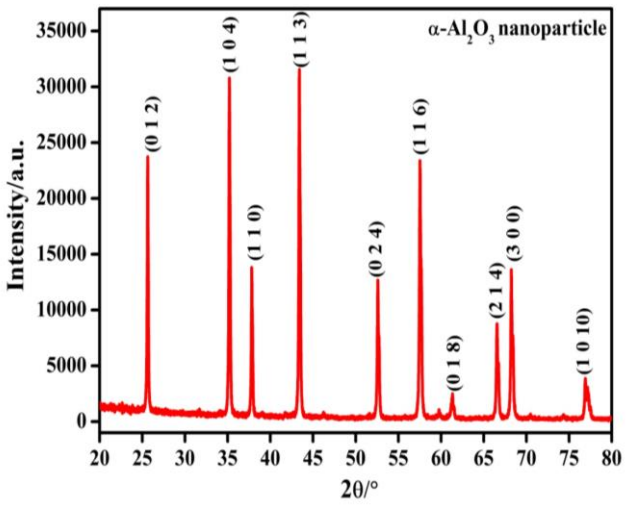

Fig.2. Powder X-ray diffraction pattern of alumina particles at the calcination temperature of 1150 °C for 3 hrs.

An XRD result reveals the presence of Bragg's peak at different angles 2Θ (°) ~ 25.4°,35.0°, 37.7°, 43.8°, 52.5°, 57.4°, 61.5, 66.5°, and 68.1°, respectively with lower and higher intensity. The diffraction peaks at respective angles are related to the corresponding planes (0 1 2), (1 0 4) (1 1 0) (1 1 3) (0 2 4), (1 1 6), (0 1 8), (2 1 4), (3 0 0), (1 0 10), respectively. All these diffraction peaks with the respective angle is consistence with the presence of crystalline nature of the α-Al_2O_3 nanoparticles in pure phase and the existence of hexagonal structure (Space Group: R-3c) which is justifies by ICDD card number 01-081-2267 [Preparation and investigation of the structural properties of α-Al_2O_3 nanoparticles using sol-gel method]. Moreover, the value of lattice parameters

Journal of Chemical Health Risks

www.jchr.org

JCHR (2024) 14(5), 861-866 | ISSN:2251-6727

(a, b and c) for hexagonal structure of α-Al_2O_3 nanoparticles are observed to be a=b= 4.761 Å and c= 12.978Å. The Scherrer technique was used to determine the average crystallite size of alumina nanoparticles by using peak broadening analysis of XRD in accordance with equation (1) [17].

$$\mathbf{D}=\frac{k\lambda}{\beta cos\theta} \qquad \textbf{-} \quad \textbf{(1)}$$

Here, β, θ and k represents the full width at half maximum (FWHM), Bragg's diffraction angle, and the shape factor. The wavelength of the X-ray landing on the sample is represented by λ. The values of average crystallite of Al_2O_3 NPs calculated using Eq. (1) and are mentioned in Table. 1

Furthermore, it is important to remember that the Scherrer equation has limitations when it comes to precisely calculating size since it fails to take into account the strain that faults or imperfections develop in the lattice. Consequently, in order to precisely estimate the size of the NPs, further techniques are required, and the Williamson–Hall plot is used for this purpose. As a result, additional techniques are required to precisely estimate the size of the NPs, which is done using the Williamson–Hall plot. The W-H plot of synthesized Al_2O_3 NPs at the calcination temperature of 1150 ºC for 3 hrs as depicts in the Fig. 2

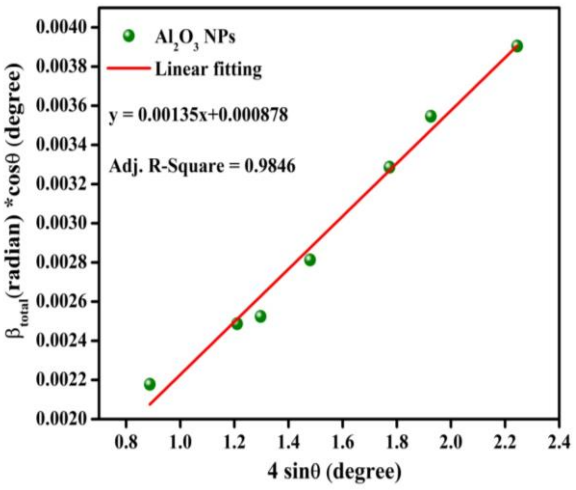

Fig.3 Plot of $\beta_{total} * cos\theta$ against 4 $sin\theta$ of synthesized α-$A_{l2}O_3$ nanoparticles.

The value of average crystallite size (D) and the micro-strain (ε) are obtained through intercept (c) and slope (m) of the curve by plotting 4 Sinθ on x-axis and β_{total}*cosθ, using the following equation (2) [18]

$$\boldsymbol{\beta_{total} * cos\theta = \frac{K\lambda}{D} + 4\varepsilon\, sin\theta} \qquad \textbf{-} \quad \textbf{(2)}$$

The intercept (c=$\frac{K\lambda}{D}$) and slope (m=ε) were obtained by comparing the equation (2) with y = c + mx. The value intercept and slope computed from the curve and comes to be 0.000878 and 1.35×10^{-3}, respectively. The respective value of D and ε for alumina nanoparticles was estimated using intercept and slope values to be 157.85 nm and 1.35×10^{-3}.

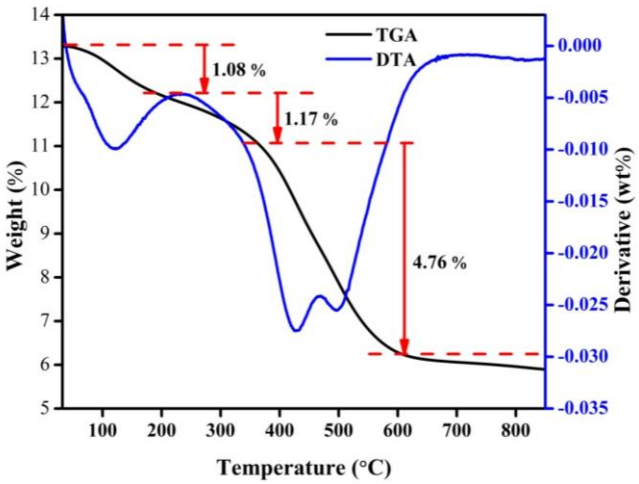

Fig.4 The plot of TGA and DSC curve against temperature range of RT to 850 ◦C.

The plot of TGA and DSC curve against temperature range of RT to 850 ◦C for identification of weight loss (%) and heat flow of alumina nanoparticles as depicts in Fig. 4. The figure reveals the presence of three different mass-stages corresponding to temperature around 190 ◦C, 336 ◦C and around 608 ◦C, respectively. First, the DSC plot shows an endothermic peak at about 115 ◦C, which is due to the loss of extra water and acetic acid and there is also appearance of weight loss of 1.08 % estimated in the range from RT to 200 ◦C. The broad endothermic peaks that occur at 428 ◦C may be associated to the dehydration reaction of the citrate precursor, and the second weight loss of 1.17 wt% emerges in the 200–350 ◦C range [19]. The final weight loss observed to be 4.76 % corresponding to the temperature after 800 ◦C with the endothermic peaks appear around at 495 ◦C, showing increase in thermal stability of the nanoparticles which is important for any future

Journal of Chemical Health Risks

www.jchr.org

JCHR (2024) 14(5), 861-866 | ISSN:2251-6727

industrial applications, such high-temperature catalysis and the creation of biomaterials [20].

Scanning electron microscopy (SEM) was used to perform surface morphological investigations of the alumina NPs on the scale of 1µm as seen in Fig. 5(a). The grains with unclear grain boundaries present in the SEM micrograph are in deformed shape with the sharp edges as clearly inferring from figure [21]. The existence of compact structure of grain are seen, results indicates the lower porosity and the average grain size is observed to be 1.01 µm by using Image J software. The estimated value of average grain size through Image J software is similar to the results obtained from histogram plot represented by Fig. 5(b). The similar nature of grains was seen in the cross-sectional SEM image measured on the 50 µm scale to that of SEM results with the average grain size of 7.43 µm as shown in Fig. 5(c).

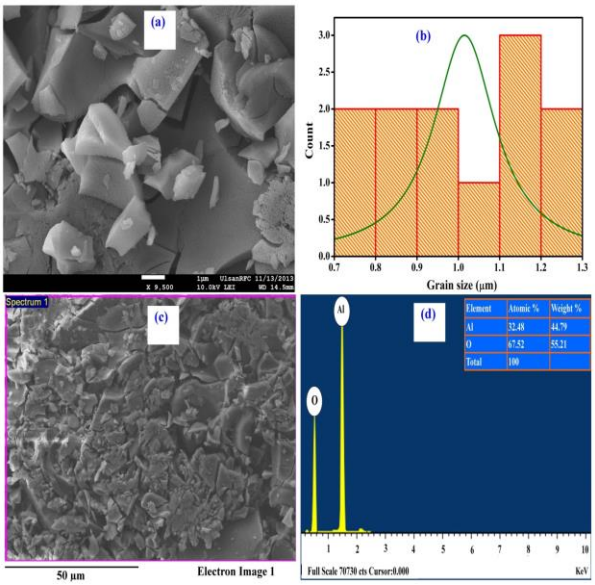

Fig. 5- EDS pattern of the sample shows the purity of the materials.

Fig. 5(d) exhibits the EDS pattern of the sample inferred the presence of Al, O elements without any other impurity elements with the Atomic and weight percentage as disclosed in the inset of figure, emphasized the stoichiometry and purity of the materials.

4. Conclusions

This work effectively reported the creation of CuO nanoparticles utilizing Sol-Gel approach for 5 hours at the temperature required for calcination of 1150 °C. XRD results verified hexagonal structure of α-alumina NPs without any other extra impurity. The lattice parameters corresponding to the hexagonal phase of the NPs were found to be a = b = 4.761 Å and c= 12.978Å. The average crystallite size (D) and micro-strain (ε) estimated through W-H plot were determined to be 157.85 nm and 1.35×10^{-3}, respectively. Using Image J software to compute the average grain size of the CuO Nps from SEM and from cross-sectional SEM images was to be 1.01 µm and 7.43 µm, respectively. The presence of the appropriate elements, Al and O in the alumina NPs verified the purity of the materials.

ACKNOWLEDGEMENTS

Authors are grateful to the concerned authorities of respective.

References

[1] H. Noda, K. Muramoto, H. Kim, Preparation of nano-structured ceramics using nanosized Al_2O_3 particles, J. Mater. Sci. 38 (2003) 2043–2047.

[2] S. Kim, J.J. Gislason, R.W. Morton, X.Q. Pan, H.P. Sun, R.M. Laine, Liquid-feed flame spray pyrolysis of nanopowders in the alumina-titania system, Chemi. Mater. 16 (12) (2004) 2336–2343.

[3] B. Kumar , R. K. Thareja, Synthesis of aluminum oxide nanoparticles using laser ablation in liquid, Phys. Status Solidi C 7(5), 1409–1412 (2010)

[4] W. J. Zhang, X. L. Wu, J.Y. Fan, G. S. Huang, T. Qiu, and P. K. Chu, Luminescent amorphous alumina nanoparticles in toluene solution, J. Phys.: Condens. Matter 18, 9937 (2006).

[5] Y. Liu, Z.-F. Zhang, J. Halloran and R. M. Laine, "Yttrium Aluminum Garnet Fibers from Metalloorganic Precursors", J. Am. Ceram. Soc., 81 (1998) 629.

[6] R. Pampuch, An Introduction to Ceramics 95 (2014).

[7] M. Kaur, S. Ishii, S.L. Shinde, T.N. Laxman, All-ceramic solar-driven water purifier based on anodized aluminum oxide and plasmonic titanium nitride, Adv. Sustain. Syst. 3(2) (2018) 1–8.

Journal of Chemical Health Risks

www.jchr.org

JCHR (2024) 14(5), 861-866 | ISSN:2251-6727

[8] V.D. Kingery, H.K. Bowen, D.R. Ublmann, "Introduction to Ceramics", 2nd ed Wiley Series on the Science and Technology of Materials, 1975.

[9] M.H. Zare, N. Hajilary, M. Rezakazemi, Microstructural modifications of polyethylene glycol powder binder in the processing of sintered alpha alumina under different conditions of preparation, Mater. Sci. Energy Technol. 2 (2019) 89–95.

[10] M.H. Mert, M.S. Mert, Preparation and characterization of encapsulated phase change materials in presence of γ –alumina for thermal energy storage applications, Thermochem. Acta 681 (2019) 1–10.

[11] B.S. Inbaraj, B.H. Chen, Y.C. Rajan, 'Synthesis and characterization of poly(γ-glutamic acid)-based alumina nanoparticles with their protein adsorption efficiency and cytotoxicity towards human prostate cancer cells', RCS Adv. 5 (2015) 15126.

[12] H.R. Ghorbani, 'A review of methods for synthesis of Al nanoparticles', Orient. J. Chem. 30(4) (2014) 1941–1949.

[13] S.N. S. Mohamad , N. Mahmed, D. S. C. Halin, K. A. Razak, M. N. Norizan, I.S. Mohamad, Synthesis of alumina nanoparticles by sol-gel method and their applications in the removal of copper ions (Cu^{2+}) from the solution, Materials Science and Engineering 701 (2019) 012034,

[14] J. Li, P. Yubai, X. Changshu, G. Qiming, G. Jingkun, "Low temperature synthesis of ultrafine α-Al_2O_3 powders by a simple aqueous sol-gel process." Ceram. Int. 32(5) (2006) 587-591.

[15] S.M. Kim, Y.J. Lee, K.W. Jun, J.Y. Park, H.S. Potdar, synthesis of thermo-stable high surface area alumina powder from sol-gel derived boehmite, Mater. Chem. Phys. 104(1) (2007) 56-61.

[16] Z. Hosseini, M. Taghizadeh, F. Yaripour, synthesis of nanocrystalline γ - Al2O3 by sol-gel and precipitation methods for methanol dehydration to dimethyl ether, J. Nat. Gas Chem. 20(2) (2011)128-134.

[17] A. Kumar, S. S. Yadava , L. Singh, M. K. Verma , N.B. Singh , K.D. Mandal, Enhancement of dielectric and magnetic properties of $0.5BaFe_{12}O_{19}$-$0.5Bi_{2/3}Cu_3Ti_4O_{12}$, J. Magn. Magn. Mater. 527(2021) 167807.

[18] Anuj Kumar Gond, Atendra Kumar, Himanshu Shekher, Anees A. Ansari, Hye-Won Seo, KD Mandal, Youngil Lee and Laxman Singh, Fabrication and Physiochemical Characterization of Zinc Oxide Nanoparticles via Citric Assisted Auto Combustion Synthesis, Current nanomaterials (2023): http://dx.doi.org/10.2174/012405461525553723092005103 7

[19] Atendra Kumar, Shiva Sundar Yadava, Laxman Singh , Manish Kumar Verma , N.B. Singh , K.D. Mandal, Enhancement of dielectric and magnetic properties of $0.5BaFe_{12}O_{19}$-$0.5Bi_{2/3}Cu_3Ti_4O_{12}$ nanocomposite synthesized via chemical route

[20] S. Ali, Y. Abbas, Z. Zuhra, I.S. Butler, synthesis of γ-alumina (Al_2O_3) nanoparticles and their potential for use as an absorbent in the removal of methylene blu dye from industrial wastewater, Nanoscale Advances 1(1), (2019) 213-218.

[21] J. Nalaskowski, M. Niewiadomski, V.K. Paruchuri, J.D. Miller, characterization of spherical alumina particles obtained by melting in a Hydrogen-oxygen flame Society for Mining, Mettalurgy, and Exploration, Littleton.2003.